On the synchrony of morphological and molecular signaling events in cell migration

Justin Dauwels[•†*], Yuki Tsukada[•+‡], Yuichi Sakumura[+‡], Shin Ishii[+‡#], Kazuhiro Aoki[#], Takeshi Nakamura[#], Michiyuki Matsuda[#], François Vialatte[*], and Andrzej Cichocki[*]

[•]These authors contributed equally
[†]Massachusetts Institute of Technology, Cambridge, MA
[*]RIKEN Brain Science Institute, Saitama, Japan
[+]Nara Institute of Science and Technology (NAIST), Nara, Japan
[#]Kyoto University, Kyoto, Japan
[‡]Institute for Bioinformatics Research and Development (BIRD), Japan Science and Technology Agency (JST).
jdauwels@mit.edu, {yuki-ts,saku}@is.naist.jp
{ishii@i,kaoki@path1.med,tnakamr@lif,matsudam@path1.med}.kyoto-u.ac.jp
{fvialatte,cia}@brain.riken.jp

Abstract. This paper investigates the dynamics of cell migration, which is the movement of a cell towards a certain target area. More specifically, the objective is to analyze the causal interdependence between cellular-morphological events and molecular-signaling events. To this end, a novel data analysis method is developed: first the local morphological changes and molecular signaling events are determined by means of edge evolution tracking (EET), next the interdependence of those events is quantified through the method of stochastic event synchrony (SES).
The proposed method is applied to time-lapse fluorescence resonance energy transfer (FRET) images of Rac1 activity in motile HT1080 cells; the protein Rac1 is well known to induce filamentous structures that enable cells to migrate. Results show a significant delay between local Rac1 activity events and morphological events. This observation provides new insights into the dynamic relationship between cellular-morphological change and molecular-signaling of migrating cells, and may pave the way to novel biophysical models of cell migration.

1 Introduction

In recent years, a wide variety of high-throughput approaches for biological experiments has emerged. Such experiments not only generate a vast amount of data, in addition, the scientific questions addressed through that data are often non-standard, and require entirely novel data analysis techniques. A prime example is micro-array data in genomics and proteomics.

In this paper, we deal with a similar example, i.e., live cell imaging data; this data allows us to gain more insight into the dynamics of cellular mechanisms. In particular, we investigate *cell migration*, which is the movement of a cell towards a certain target area; it is one of the central processes in the development and maintenance of multicellular organisms. For example, tissue formation during embryonic development, wound healing and immune responses all require the orchestrated movement of cells in a particular direction to a specific location.

Errors during this process have serious consequences, including mental retardation, vascular disease, tumor formation and metastasis. Despite the obvious importance, the dynamics behind cell migration are poorly understood. Such understanding may lead to the development of novel therapeutic strategies for controlling, for instance, invasive tumor cells [1]. Although the recent advancement of both molecular biology and the technique of live cell imaging shed some light on the mechanisms of cellular morphological regulation [2, 3], and in parallel, some computational methods for quantitative analysis of time-lapse images have been developed (see, e.g., [4]), there remains a wide variety of computational challenges. One of those challenges is to analyze the interdependence of different kinds of events in time-lapse images of cells during cell migration.

In this study, we analyze *fluorescence resonance energy transfer* (FRET) images of Rac1 in motile HT1080 cells, which are human fibrosarcoma cells [7]. The protein Rac1 is well known to induce filamentous structures that enable cells to migrate. We analyze the statistical relation between Rac1 activity events and morphological events. For this purpose, we develop a novel computational method for quantifying those interdependencies. This method consist of two steps:

1. We first determine the morphological and molecular activity events from the time-lapse microscopy images. To this end, we apply *edge evolution tracking* (EET) [5]: it identifies cellular-morphological events and molecular-activity events, and determines the distance in space between those events, taking the evolution of the cell morphology into account.
2. Next we quantify the interdependence between those morphological and activity events by means of *stochastic event synchrony* (SES) [6]: using the EET distance measure, SES tries to align cellular morphological with molecular activity events; the better this alignment can be carried out, the more similar the event sequences are considered to be. In addition, the method is able to determine delays between both event sequences.

This paper is organized as follows. In the next section, we describe the the edge evolution tracking (EET) method; in Section 3, we briefly review the stochastic event synchrony (SES) method. In Section 4, we combine those two methods to analyze live cell FRET data of Rac1 in motile HT1080 cells. In Section 5, we discuss our results, and in Section 6, we offer some concluding remarks.

2 Edge Evolution Tracking

In earlier work [5], we developed an algorithm, referred to as *edge evolution tracking* (EET), to quantify the dynamics of local cell morphological changes from FRET images. The method focusses on local *area* change instead of local *structural* change as morphological property. As a consequence, EET does not make a clear distinction between structural differences such as filopodia and lamellipodia. However, such distinction is not required in the current study, and EET is therefore suitable for our purposes.

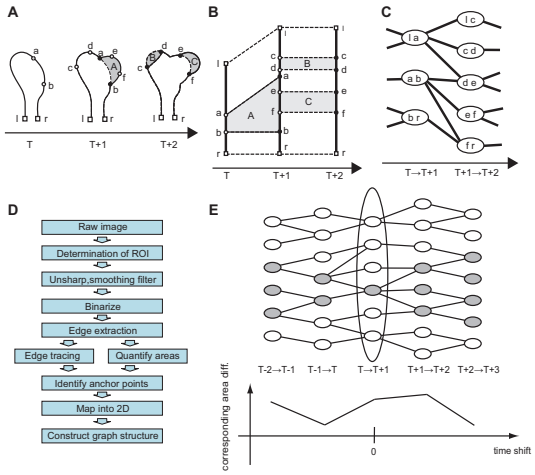

Fig. 1. Edge evolution tracking. (A) Cell boundary, anchor points a-f and area differences A-C from T to $T+2$. The points l and r denote terminals of the boundary; (B) Segment transition diagram; (C) Non-vanishing segment graph; (D) Flow chart of EET; (E) Evolution of particular (non-vanishing) segment over time.

2.1 Principle

EET divides the cell edge boundaries in segments, and tracks how those segments evolve over time. By tracking boundary segments, one can identify which segments protrude, retract, or remain at the same position. The EET method consists of the following steps:

1. As a first step, the time-lapse microscopy images are preprocessed: we apply a smoothing filter, and next we threshold the pixel intensities, resulting in binary images. From those binary images, we extract the cell boundaries.
2. The cell boundaries are divided into segments (see Fig. 1A). The boundary points of each segment are identified as "anchor points" (lowercase letters in Fig. 1A). Those anchor points often separate parts of the boundary that protrude, retract, or remain unchanged. We also determine the center of each segment and its width.
3. We determine the correspondence between segments of consecutive time instances (see Fig. 1B). Some segments vanish in the next time instance, others remain. For example, segment $[a, e]$ disappears in the transition from $T+1$ to $T+2$. Non-vanishing segments may either grow, shrink, or remain unchanged as they evolve to the next time instance. In the segment-transition diagram of Fig. 1B, the anchor points of non-vanishing segments at consecutive time instances are interconnected by dotted lines, and the associated area differences are labeled. The sequence of non-vanishing segments may be represented by a graph structure as depicted in Fig. 1C. Each node represents a non-vanishing segment. Two segments at consecutive time instances are connected if they overlap.

A flow chart of the EET procedure is shown in Fig. 1D.

Once the EET method has been applied, one can compute several interesting quantities. For example, it allows us to investigate the evolution of a particular segment over time, using the graph of Fig. 1C. As an illustration, Fig. 1E (top) shows the time course of the colored non-vanishing segment at transition $T \to T+1$; more specifically, it depicts all corresponding segments before T and after $T+1$ (colored in grey). Fig. 1E (bottom) shows how the area differences of that family of corresponding segments vary over time. Obviously, one may analyze all other nodes of Fig. 1E (top) in a similar fashion.

We wish to point out that the parameters of the preprocessing step affect the results of EET. However, those results are consistent once the preprocessing parameters have been determined, even if the cells show strongly time-varying behavior.

2.2 Morphological and Activity Events

Activity events A_k are defined as follows. First one computes the local activity along each *point* P of the cell boundary; it is defined as the average intracellular FRET value inside a circle with center at P and radius R. The local activity of a *segment* is defined as the average of the local activity within that segment. If the local activity of a particular (non-vanishing) segment is *larger* than a certain threshold θ_{ac}, we say that an activity event (" activity burst") has occurred at that segment of the cell boundary. In principle, one may define activity dips in a similar fashion. In this paper, however, we will merely consider activity bursts.

Morphological events $M_{k'}$ are extracted from the area differences. If the area difference of a particular (non-vanishing) segment is *larger* than a certain (positive) threshold θ_{ar}, we say that a morphological event has occurred at that segment of the cell boundary, in particular, a protrusion event. In principle, one may define retraction events in a similar fashion. In this paper, however, we will only study protrusion: more specifically, we wish to investigate how activity bursts are related to protrusion events.

Each event A_k and $M_{k'}$ is described by four parameters: (i) occurrence time; (ii) location on the cell boundary, which is given by the center of the corresponding segment; (iii) width, which is defined as length of the corresponding segment; (iv) amplitude (either local activity or area difference).

2.3 Spatial Distance Between Activity and Morphological Events

In order to define the spatial distance between activity and morphology events A_k and $M_{k'}$ respectively, we make use of the diagrams obtained through EET analysis. If both events occur at the same time instance, their distance is defined as the curve length of the shortest path *within the cell* that connects the two events. The shortest path is not necessarily a straight line, and the distance between A_k and $M_{k'}$ is in general non-euclidean. If the events A_k and $M_{k'}$ occur at different time instances, we first identify the segments $\tilde{M}_{k'}$ corresponding to $M_{k'}$ at the time frame of A_k. Since the segments $\tilde{M}_{k'}$ are neighboring, they can be treated as one "large" segment. We use segments $\tilde{M}_{k'}$ at time frame of A_k and not vice versa, since the boundary segments are defined based upon morphological characteristics. Eventually, the distance between A_k and $M_{k'}$ is defined as the distance between A_k and $\tilde{M}_{k'}$, i.e., the length of the shortest path *within the cell* that connects A_k with the center of $\tilde{M}_{k'}$.

3 Stochastic Event Synchrony

In earlier work [6], we developed a method to quantify the interdependence of two event sequences ("point processes"), referred to as *stochastic event synchrony* (SES). We will first briefly describe SES in the context of the application considered in [6], i.e., point processes in time-frequency domain. Next we outline how SES can be applied to morphological and activity events.

3.1 Bump Models in Time-Frequency Domain

In [6], one wishes to determine the similarity of pairs of signals (e.g., EEG signals). The latter are first transformed into time-frequency domain. The resulting time-frequency maps are usually sparse, and contain distinct "bumps" of activity (see Fig. 2). The EEG signals are modeled as sequences of such bumps, which are event sequences in time-frequency domain [8]. The resulting bump models X and X', representing the most prominent oscillatory activity, are then aligned (see Fig. 3): bumps in one time-frequency map may not be present in the other map ("non-coincident" bumps); other bumps are present in both maps ("coincident bumps"), but appear at slightly different positions on the maps.

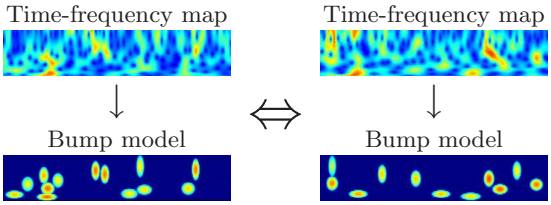

Fig. 2. Bump models. Top: time-frequency maps of the two signals; bottom: bump models extracted from the time-frequency maps.

The black lines in Fig. 3(right) connect the centers of coincident bumps, and hence, visualize the offset in position between pairs of coincident bumps. Stochastic event synchrony consists of five parameters (SES) that quantify the alignment of two bump models:

- ρ: fraction of non-coincident bumps,
- δ_t and δ_f: average time and frequency offset respectively between coincident bumps,
- s_t and s_f: variance of the time and frequency offset respectively between coincident bumps.

The parameters ρ and s_t are related to similarity, since they quantify the synchrony between bump models; low ρ and s_t implies that the two bump models at hand are well synchronized.

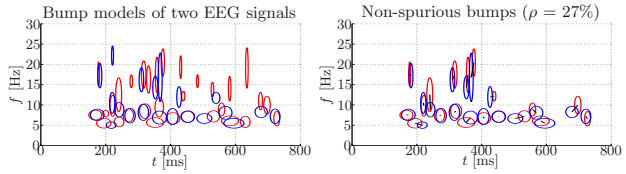

Fig. 3. Coincident and non-coincident activity ("bumps"). (left) bump models of two signals (one in red, the other in blue); (right) coincident bumps; the black lines connect the centers of coincident bumps.

The alignment of the two event sequences (cf. Fig. 3 (right)) is cast as a statistical inference problem [6]. The associated probabilistic model depends on the SES parameters $\theta = (\delta_t, \delta_f, s_t, s_f)$ besides the following two kinds of latent variables: (i) binary variables $C_{kk'}$, associated to each pair of bumps X_k and $X'_{k'}$, where $C_{kk'} = 1$ indicates that event X_k is coincident with event $X'_{k'}$, and where $C_{kk'} = 0$ otherwise; (ii) binary variables B_k and $B'_{k'}$, where $B_k = 1$ and $B'_{k'} = 1$ indicate that X_k and $X'_{k'}$ respectively are non-coincident. The latent-variable model is of the form:

$$
\begin{aligned}
p(x, x', b, b', c, \theta) \propto & \prod_{k=1}^{n} (\beta\delta[b_k - 1] + \delta[b_k]) \prod_{k'=1}^{n'} (\beta\delta[b'_k - 1] + \delta[b'_k]) \\
& \cdot \prod_{k=1}^{n} \prod_{k'=1}^{n'} \Big(\mathcal{N}(t'_{k'} - t_k; \delta_t, s_t) \mathcal{N}(f'_{k'} - f_k; \delta_f, s_f) \Big)^{c_{kk'}} \\
& \cdot \prod_{k=1}^{n} \big(\delta[b_k + \sum_{k'=1}^{n'} c_{kk'} - 1]\big) \prod_{k'=1}^{n'} \big(\delta[b'_{k'} + \sum_{k=1}^{n} c_{kk'} - 1]\big) p(\delta_t) p\big(s_t\big) p(\delta_f) p\big(s_f\big), \quad (1)
\end{aligned}
$$

where β is a constant, n and n' is the total number of bumps in X and X' respectively, and $\mathcal{N}(x; m, s)$ stands for a univariate Gaussian distribution with mean m and variance s [6]. Note that the Gaussian factors in (1) correspond to an *euclidean* metric in the time-frequency domain. For convenience, we choose improper priors $p(\delta_t) = 1 = p(\delta_f)$ and conjugate priors $p(s_t)$ and $p(s_f)$. The SES parameters $\theta = (\delta_t, \delta_f, s_t, s_f)$ and the latent variables C, B and B' are determined jointly by MAP estimation; we refer to [6] for more details.

3.2 Events in Cell Migration

Instead of two bump models X and X', we now have an activity event sequence A and a morphological event sequence M. The events in those sequences also have two coordinates: time t and position u along the cell boundary; the parameters δ_f and s_f are replaced by δ_u and s_u. There are two important differences with the previous application: (1) the timing offset δ_t is no longer (almost) zero; (2) the distance between events is no longer euclidean, since it is computed based upon the EET graph (cf. Section 2.3). The factor $\mathcal{N}(f'_{k'} - f_k; \delta_f, s_f)$ in (1) is replaced by $\mathcal{N}(g(t_k, u_k, t'_{k'}, u'_{k'}); \delta_u, s_u)$, where g corresponds to the EET distance measure, and t, t', u, and u' are the occurrence times and positions of the activity events A and morphological events M respectively.

4 Application

We applied our methods to the fluorescence resonance energy transfer (FRET) images of motile HT1080 cells, which are human fibrosarcoma cells [7]. More precisely, FRET technique was used for monitoring activity of *Rac1*; the latter is a member of Rho family small GTPases (see previous studies on FRET imaging, e.g., [5]). Rho GTPases act as binary switches by cycling between inactive and active states, and play a key role in linking biochemical signaling with biophysical cellular behaviors; this is achieved mainly through reorganization of the actin and

microtubule cytoskeleton. In particular, Rac1 is well known to induce specific filamentous actin structures called *lamellipodia*.

The data set consists of 3 FRET movies; each movie is recorded from a different HT1080 cell, has a time-lapse (frame-rate) of 1 frame per minute, and lasts about 30 minutes. The HT1080 cells were uniformly stimulated with nerve growth factor, 24 hours before the movies were recorded. The cells showed spontaneous migration during the recording.

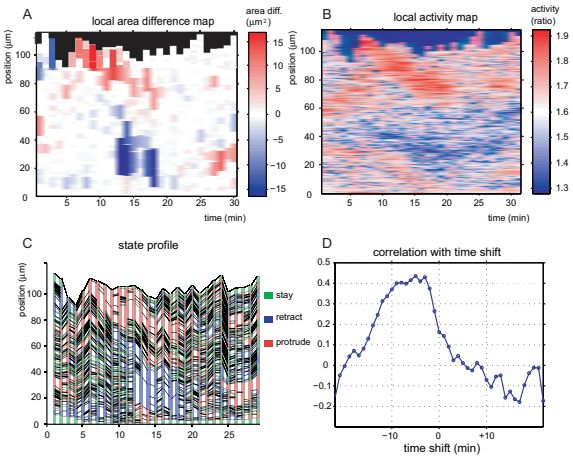

Fig. 4. Results of EET. (A) Area difference values; (B) Activity values; (C) Local morphological status. Red, blue and green denote protrusion, retraction and pause, respectively; (D) Cross-correlation between area difference and activity map.

5 Results and Discussion

First we applied EET to the FRET time-lapse images in order to determine the morphological and molecular-signaling events. This procedure resulted in the area difference map, activity map, and state profile for each of the three FRET movies. Figs. 4 illustrates those three maps for one of the analyzed movies (A, B, and C respectively). In each of the three maps, the horizontal and vertical axis represent time and position along the boundary respectively. The area difference map (see Fig. 4A) and local activity map (see Fig. 4B) depict the area difference and local activity respectively for each (non-vanishing) segment of the cell boundary as a function of time. The state profile (see Fig. 4C) depicts the morphological state of each (non-vanishing) segment of the cell boundary as a function of time. The morphological and molecular-signaling events were extracted from the area difference and local activity map respectively by thresholding (with thresholds θ_{ar} and θ_{ac} respectively).

Next we applied the stochastic event synchrony (SES) method in order to analyze the interdependence between morphological events and activity events. For reasonable values of the thresholds θ_{ar} and θ_{ac}, activity kernel radius R, parameter β, we found that the delay δ_t between morphological events and activity events is negative; in other words, on average the morphological events occur first, followed by activity events. We observed this in each of the three movies.

As an alternative approach, we calculated cross-correlation between the area difference and the activity map (see Fig. 4D), as in a previous study [5]. The cross-correlation shows high correlation at negative time-shifts, in agreement with the SES analysis. However, it is hard to extract a precise value for the delay from the cross-correlation function shown in Fig. 4D, since the peak is wide. On the other hand, SES yields more precise estimates of delay, i.e., the parameter δ_t; the uncertainty in δ_t is quantified by σ_t, the standard deviation of the timing jitter, more precisely, by the ratio $|\delta_t|/\sigma_t$; the latter is significantly larger than 1 in the application at hand, and hence, the estimate δ_t can be considered reliable.

6 Conclusion

We studied the dynamics of cell migration, particularly, we analyzed the causality between cellular-morphological events and molecular-signaling events. To this end, we developed a novel data analysis method that blends edge evolution tracking (EET) with the method of stochastic event synchrony (SES).

We used that method to study time-lapse fluorescence resonance energy transfer (FRET) images of Rac1 activity in motile HT1080 cells; our results indicate that local Rac1 activity events are delayed w.r.t. morphological events. This seems to suggest that the cell first changes its shape, probably as a random fluctuation, and next there is an influx of Rac1, most likely required to *sustain* that morphological change. Obviously, further investigations are required to unravel the underlying molecular mechanisms.

In future work, we will apply our method to a large number of FRET movies in order to confirm our findings. In addition, we will incorporate more detailed biophysical processes into our method, which should allow us to refine our observations.

References

1. D. A. Lauffenburger and A. F. Horwitz, "Cell migration: a physically integrated molecular process," *Cell* **84** (1996) 359–369.
2. D. Dormann and C. J. Weijer, "Imaging of cell migration," *The EMBO Journal* **25** No. 15 (2006) 3480–3493.
3. T. D. Pollard, "The cytoskeleton, cellular motility, and the reductionist agenda," *Nature* **422** (2003) 741–745.
4. D. Gerlich, J. Mattes, and R. Eils, "Quantitative motion analysis and visualization of cellular structures," *Methods* **29** (2003) 3–13.
5. Y. Tsukada, K. Aoki, T. Nakamura, Y. Sakumura, M. Matsuda, and S. Ishii, "Quantification of local morphodynamics and local GTPase activity by edge evolution tracking," submitted.
6. J. Dauwels, F. Vialatte, T. Rutkowski, and A. Cichocki, "Measuring neural synchrony by message passing," *Advances in Neural Information Processing Systems 20,* MIT Press.
7. S. Rasheed, W.A. Nelson-Rees, E.M. Toth, P. Arnstein, M.B. Gardner, "Characterization of a newly derived human sarcoma cell line (HT-1080)," *Cancer* **33** (1974) 1027–33.
8. F. Vialatte, C. Martin, R. Dubois, J. Haddad, B. Quenet, R. Gervais, and G. Dreyfus, "A machine learning approach to the analysis of time-frequency maps, and its application to neural dynamics," *Neural Networks* **20**, 194–209.